Electronic Supplementary Information

Multicolor fluorescence encoding of different microRNAs in lung cancer tissues at single-molecule level

Chen-chen Li,[‡,ab] Hui-yan Chen,[‡,a] Xiliang Luo,*[,b] Juan Hu*[,c] and Chun-yang Zhang*[,a]

[a] College of Chemistry, Chemical Engineering and Materials Science, Collaborative Innovation Center of Functionalized Probes for Chemical Imaging in Universities of Shandong, Key Laboratory of Molecular and Nano Probes, Ministry of Education, Shandong Provincial Key Laboratory of Clean Production of Fine Chemicals, Shandong Normal University, Jinan 250014, China. E-mail: cyzhang@sdnu.edu.cn

[b] Key Laboratory of Optic-electric Sensing and Analytical Chemistry for Life Science, MOE, Shandong Key Laboratory of Biochemical Analysis, College of Chemistry and Molecular Engineering, Qingdao University of Science and Technology, Qingdao 266042, China. E-mail: xiliangluo@qust.edu.cn

[c] School of Chemistry and Chemical Engineering, Southeast University, Nanjing 211189, China. E-mail: hujuan@seu.edu.cn

* Corresponding author.

‡ These authors contributed equally.

Optimization of experimental conditions

To obtain the best assay performance, we optimized different experimental conditions including the amount of Vent (exo-) DNA polymerase, the amount of Nt.BstNBI nicking enzyme, the concentrations of AP probe-155 and AP probe-21, the amount of APE1, the concentrations of Cy5-dCTP and Cy3-dGTP, the reaction time of RCA, and the amount of phi29 DNA polymerase. We investigated the influence of experimental conditions upon the value of F/F_0, where F and F_0 are the fluorescence intensity in the presence and absence of target miRNA, respectively. The amounts of Vent (exo-) DNA polymerase and Nt.BstNBI nicking enzyme are the crucial factors which influence the amplification efficiency of target miRNA-induced cyclic SDA reaction. As shown in Fig. S1A, the F/F_0 value enhances with the increasing amount of Vent (exo-) DNA polymerase from 0.3 to 0.5 U, and reaches the maximum value at the amount of 0.5 U, followed by the decrease beyond the amount of 0.5 U. This can be explained by that the excess amount of Vent (exo-) DNA polymerase may induce the non-specific amplification. Therefore, 0.5 U of Vent (exo-) DNA polymerase is used in the subsequent experiments. Similarly, the F/F_0 value enhances with the increasing amount of Nt.BstNBI from 1 to 2 U, and reaches the maximum value at the amount of 2 U (Fig. S1B). Thus, 2 U of Nt.BstNBI is used in the subsequent researches.

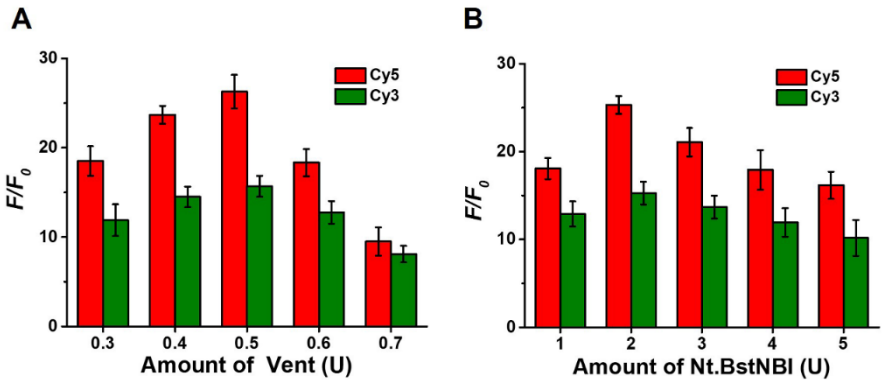

Fig. S1 (A) Variance of F/F_0 value with different amounts of Vent (exo-) DNA polymerase in the presence of miR-155 (red column) and miR-21 (olive column), respectively. (B) Variance of F/F_0 value with different amounts of Nt.BstNBI nicking enzyme in the presence of miR-155 (red column) and miR-21 (olive column) , respectively. Error bars show the standard deviation of three experiments.

The efficient APE1-assisted cyclic cleavage of AP probes may generate primers for successful RCA, and thus the concentration of AP probes and the amount of APE1 should be optimized. As shown in Fig. S2A, the F/F_0 value for miR-155 assay enhances with the increasing concentration of AP probe-155 from 80 nM to 160 nM, followed by

decrease beyond the concentration of 160 nM. Therefore, 160 nM AP probe-155 is used in the subsequent researches. Similarly, the F/F_0 value for miR-21 assay enhances with the increasing concentration of AP probe-21 from 80 nM to 160 nM, followed by decrease beyond the concentration of 160 nM. Therefore, 160 nM AP probe-21 is used in the subsequent researches. As shown in Fig. S2B, the F/F_0 value enhances with the increasing amount of APE1 from 0.5 U to 1 U, followed by decrease beyond the concentration of 1 U. Therefore, 1 U of APE1 is used in the subsequent researches.

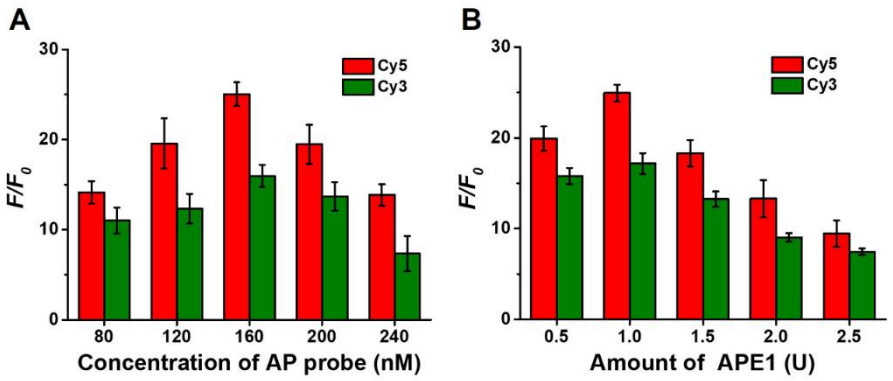

Fig. S2 (A) Variance of F/F_0 value with different concentrations of AP probe-155 (red column) and AP probe-21 (olive column), respectively. (B) Variance of F/F_0 value with different amounts of APE1 in the presence of miR-155 (red column) and miR-21 (olive column), respectively. Error bars show the standard deviation of three experiments.

Both Cy5-dCTP and Cy3-dGTP are the raw materials of RCA reaction, and their concentrations should be optimized. As shown in Fig. S3, the F/F_0 value enhances with the increasing concentrations of Cy5-dCTP and Cy3-dGTP from 4 μM to 8 μM, followed by decrease beyond the concentration of 8 μM. Therefore, 8 μM Cy5-dCTP and 8 μM Cy3-dGTP are used in the subsequent researches.

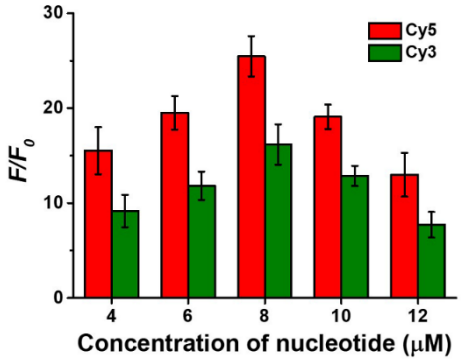

Fig. S3 Variance of F/F_0 value with different concentrations of Cy5-dCTP for miR-155 assay (red column) and Cy3-dGTP for miR-21 assay (olive column), respectively. Error bars show the standard deviation of three experiments.

We further investigated the effect of RCA reaction time and the amount of phi29 DNA polymerase upon the assay performance. As shown in Fig. S4A, the F/F_0 value enhances with reaction time from 0.5 to 1.5 h, followed by decrease beyond 1.5 h. Thus, the reaction time of 1.5 h is used in the subsequent researches. As shown in Fig. S4B, the F/F_0 value enhances with the amount of phi29 DNA polymerase from 2 to 5 U and reaches a plateau at the amount of 5 U. Therefore, 5 U of phi29 DNA polymerase is used in the subsequent researches.

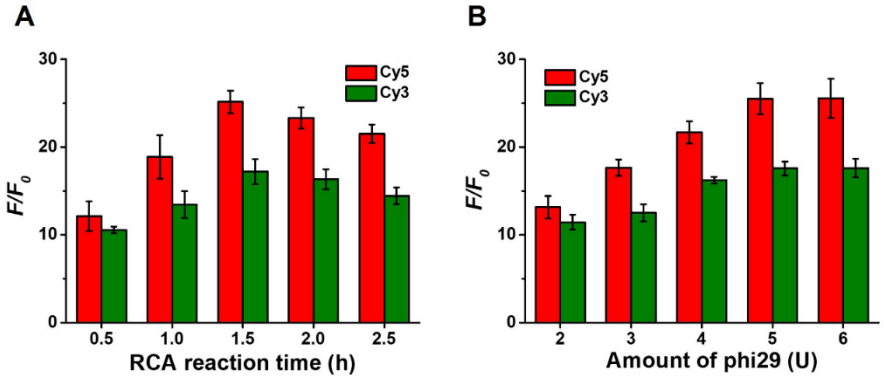

Fig. S4 (A) Variance of F/F_0 value with RCA reaction time in the presence of miR-155 (red column) and miR-21 (olive column), respectively. (B) Variance of F/F_0 value with different amounts of phi29 DNA polymerase in the presence of miR-155 (red column) and miR-21 (olive column), respectively. Error bars show the standard deviation of three experiments.

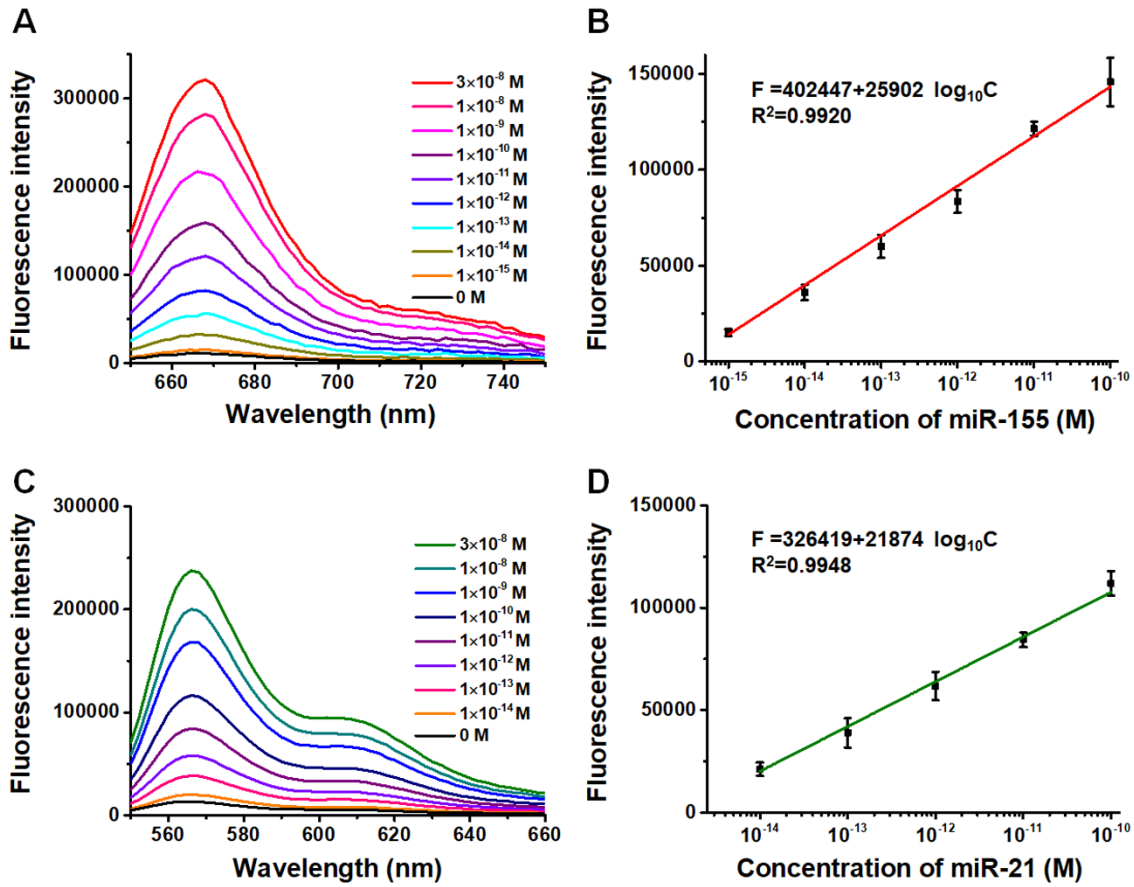

Fig. S5 (A) Cy5 emission spectra generated by different concentrations of miR-155. (B) Linear relationship between Cy5 intensity at 668 nm and the logarithm of miR-155 concentration. (C) Cy3 emission spectra generated by different concentrations of miR-21. (D) Linear relationship between Cy3 intensity at 568 nm and the logarithm of miR-21 concentration. Error bars show the standard deviations of three independent experiments.

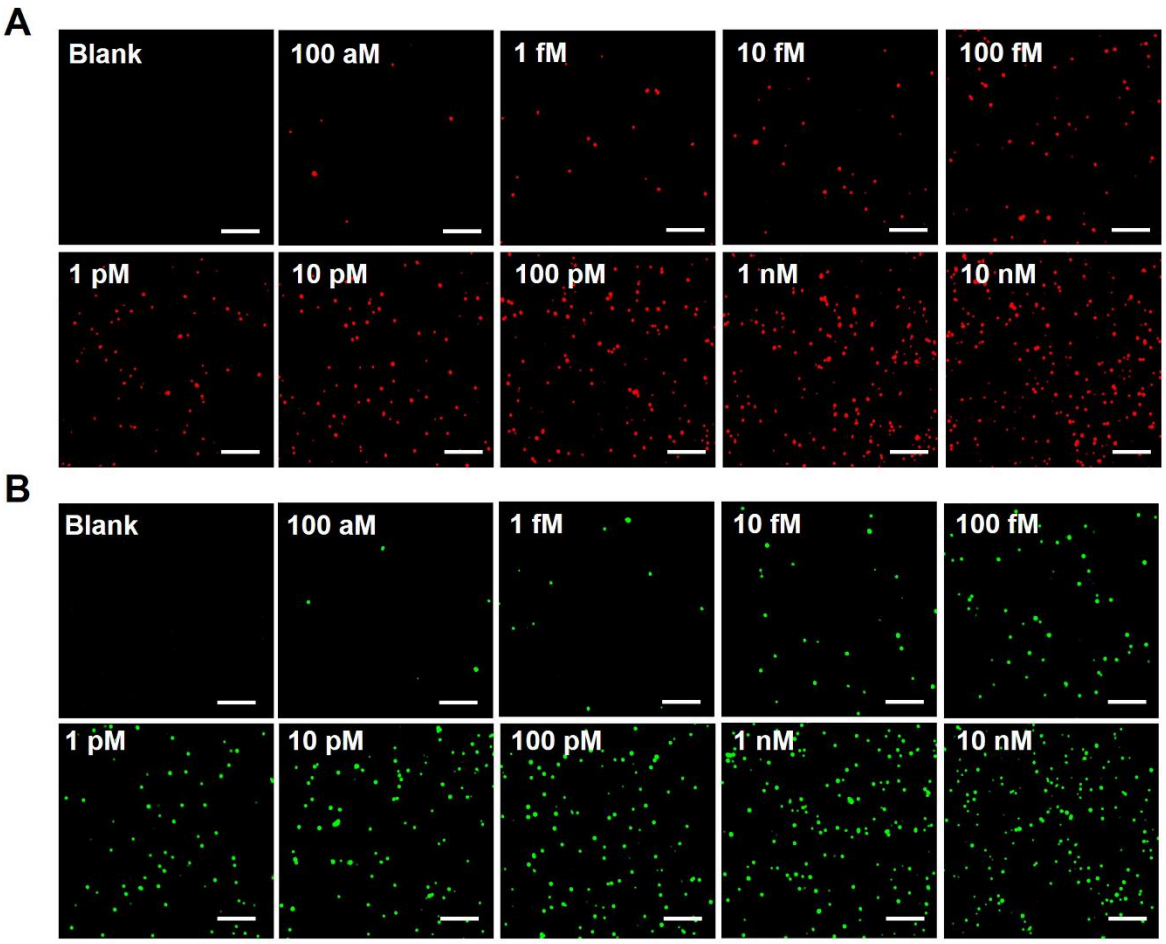

Fig. S6 Single-molecule fluorescence imaging of different-concentration miR-155 (A) and miR-21 (B). Scale bar is 5 μm.

Table S1. Comparison of the proposed method with the reported methods for miR-155 and miR-21 assays.

Analytical method	Linear range		Detection limits		Ref.
	miR-155	miR-21	miR-155	miR-21	
Bidirectional DNA walking machine-based electrochemiluminescence biosensor	5 fM – 500 pM	5 fM – 500 pM	1.67 fM	1.51 fM	1
Peptide nucleic acid-based electrochemical biosensor	50 fM – 5 nM	10 fM – 5 nM	11.63 fM	2.49 fM	2
DNA tetrahedral nanostructure-based electrochemical biosensor	10 fM – 10 nM	10 fM – 1 nM	10 fM	10 fM	3
Quantum dots and graphene oxide nano-photon switch-based fluorescent assay	1 pM – 1 nM	1 pM – 1 nM	1 pM	1 pM	4
Stir-bar assisted magnetic DNA nanospheres-encoded probes-based electrochemical assay	5 fM – 2 nM	5 fM – 2 nM	1.8 fM	1.5 fM	5
Molecular beacon-based fluorescent assay	1 nM – 50 nM	–	0.5 nM	–	6
Enzyme-free target recycling amplification and DNA tetrahedron nanoprobes-based electrochemical assay	–	0.5 fM – 100 nM	–	0.25 fM	7
Multicolor fluorophores-encoded cascade signal amplification-based fluorescent assay	1 fM – 100 pM	10 fM – 100 pM	0.983 fM	5.01 fM	This work
Multicolor fluorophores-encoded cascade signal amplification-based single-molecule detection	100 aM – 10 pM	100 aM –10 pM	25.7 aM	45.7 aM	This work

The qRT-PCR measurement

We employed qRT-PCR to verify the accuracy and reliability of the proposed method using Mir-X miRNA qRT-PCR TB Green® Kit (TaKaRa Biotechnology Co., Ltd. Dalian, China). The specific primer of miR-155 is 5' – TTA ATG CTA ATC GTG ATA GGG GT – 3', and the specific primer of miR-21 is 5' – TAG CTT ATC AGA CTG ATG TTG A – 3'. The indicated concentration of synthetic miRNAs and the total RNA extracted from real samples (cultured cell lines or lung tissues) were reverse transcribed. The PCR amplification of cDNA (the reverse transcripts of RNA) was performed under the following conditions: 95 °C for 10 s, 45 cycles of 95 °C for 5 s, and 60 °C for 20 s. The real-time fluorescence measurements were performed in a Bio-Rad CFX connect Real-Time System, and the fluorescence intensity was monitored at an interval of 25 s. Three independent experiments were performed. The synthetic miRNA oligonucleotides were used to generate standard curves for miR-155 and miR-21, respectively. As shown in Figs. S7A and S7C, the real-time fluorescence intensity enhances in a sigmoidal fashion. The threshold cycle (C_T) value exhibits a linear correlation with the logarithm of miR-155 concentration (Fig. S7B), and the regression equation is C_T = -19.63 - 3.954 $\log_{10}$ C (R^2 = 0.9979). Similarly, the C_T value exhibits a linear correlation with the logarithm of miR-21 concentration (Fig. S7D), and the regression equation is C_T = -20.78 - 3.901 $\log_{10} C$ (R^2 = 0.9960). The concentration of miRNA from real samples was calculated according to the calibration curve.

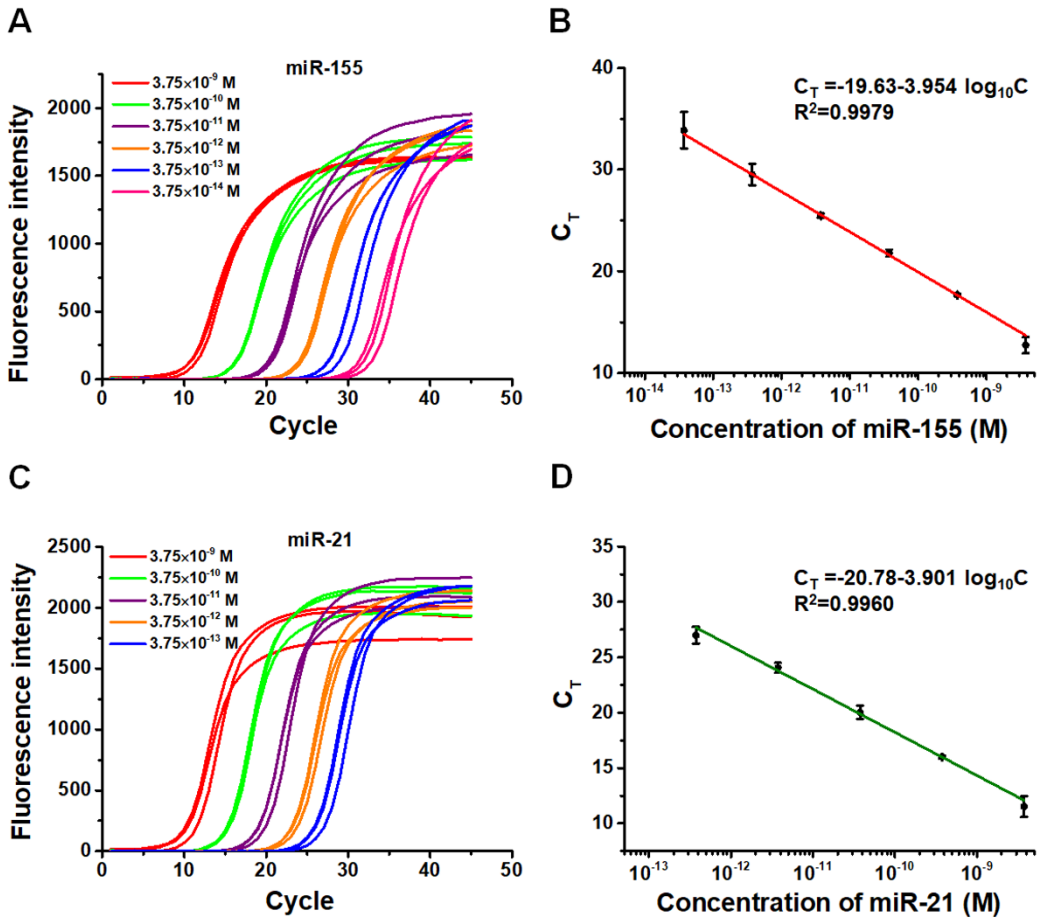

Fig. S7 Generation of calibration curve for miR-155 and miR-21 quantification by qRT-PCR. (A and C) qRT-PCR output from Bio-Rad software. (B and D) Calibration curve. Error bars show the standard deviation of three experiments.

References

1 L. Peng, P. Zhang, Y. Chai and R. Yuan, *Anal. Chem.*, 2017, **89**, 5036-5042.

2 P. Fu, S. Xing, M. J. Xu, Y. Zhao and C. Zhao, *Sens. Actuators B Chem.*, 2020, **305**, 127545.

3 D. Zeng, Z. Wang, Z. Meng, P. Wang, L. San, W. Wang, A. Aldalbahi, L. Li, J. Shen and X. Mi, *ACS Appl. Mater. Interfaces*, 2017, **9**, 24118-24125.

4 R. Huang, Y. H. Liao, X. M. Zhou, Y. Fu and D. Xing, *Sens. Actuators B Chem.*, 2017, **247**, 505-513.

5 Z. Shen, L. He, W. Wang, L. Tan and N. Gan, *Biosens. Bioelectron.*, 2020, **148**, 111831.

6 Q. Liu, J. Fan, C. Zhou, L. Wang, B. Zhao, H. Zhang, B. Liu and C. Tong, *Int. J. Anal. Chem.*, 2018, **2018**, 3625823.

7 X. L. Zhang, Z. H. Yang, Y. Y. Chang, D. Liu, Y. R. Li, Y. Q. Chai, Y. Zhuo and R. Yuan, *Chem. Sci.*, 2020, **11**, 148-153.